ChemComm

Geometrical control of the magnetic anisotropy in six coordinate cobalt complexes

Journal:	*ChemComm*
Manuscript ID	CC-COM-05-2020-003238.R1
Article Type:	Communication

COMMUNICATION

Geometrical control of the magnetic anisotropy in six coordinate cobalt complexes

Mohamed R. Saber,[a,b] Mukesh K. Singh[a] and Kim R. Dunbar[a*]

Received 00th January 20xx,
Accepted 00th January 20xx

DOI: 10.1039/x0xx00000x

The geometry of cobalt(II) ions in the axially distorted octahedral cation in $[Co(MeCN)_6](BF_4)_2$ (1) was compared to the trigonal prismatic cation in $[CoTp^{py}]PF_6$ (2) which revealed significant differences in magnetic anisotropy. Combined experimental and *ab initio* CASSCF/NEVPT2 calculations support the observed zero field SMM behaviour for 2, with easy axis anisotropy, attributed to the rigidity of the trigonal prismatic ligand. Strong transverse anisotropy for 1 leads to significant quantum tunnelling processes.

The potential applications of single molecule magnets (SMMs) in advanced technologies such as molecular spintronics and quantum computing continue to fuel activity in the field.[1-4] In recent years, considerable research effort has been directed at the exploration of magnetic anisotropy in mononuclear lanthanide and transition metal complexes.[2-4] Of specific relevance to the present report is that d^7 cobalt (II) complexes exhibit significant anisotropy and SMM properties[4-18] owing to the combined effects of spin orbit coupling and axial distortions of the crystal field.[19, 20]

In previous studies, our group demonstrated the role of axial trigonal distortion in octahedral Co(II) species for engendering significant first order unquenched orbital contributions owing to the inherent orbital degeneracy in axial coordination environments.[17] Several other groups also reported field-induced slow relaxation of the magnetization in axially distorted octahedral cobalt complexes with nitrogen and oxygen donor ligands.[21-26] The results of these combined studies underscore the importance of suppressing quantum tunneling pathways as a prerequisite for SMM behavior. Of specific interest is the fact that trigonal prismatic symmetry for Co(II) compounds leads to more efficient suppression of quantum tunneling as a result of diminished transverse anisotropy,[24] and, indeed, most reported trigonal prismatic cobalt SMM complexes exhibit SMM behavior at a zero applied field. [6-16]

Herein, we report dynamic and magneto-structural studies of the two mononuclear Co(II) complexes $[Co(MeCN)_6](BF_6)_2$ (**1**) and $[CoTp^{py}]PF_6$ (**2**) (Tp^{py} = tri(3-pyridylpyrazolyl borate, Figure 1) in axially distorted octahedral and trigonal prismatic coordination environments respectively. The electronic structures were probed using correlated electronic structure methods (CASSCF and NEVPT2) in order to gain insight into the origins of magnetic anisotropy and the relaxation properties of molecules in these two geometries.

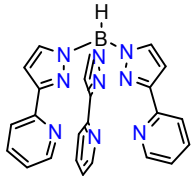

Figure 1. Tp^{py} ligand structure

Compound **1** was prepared by oxidation of cobalt powder with $NOBF_4$ in acetonitrile.[27] Diffusion of diethyl ether afforded pink-orange crystals of **1** which crystallize in the monoclinic space group $P2_1/n$ (Table S1). The cobalt center is in a low symmetry distorted octahedral environment consisting of six nitrogen atoms from coordinated acetonitrile ligands with bond lengths Co-N(1) = 2.126(4), Co-N(2) = 2.123(4), Co-N(3) = 2.104(4), Co-N(4) = 2.102(4), Co-N(5) = 2.105(4) and Co-N(6) = 2.119(4) (Figure 2, Figure S1, Table S2). The local symmetry around the cobalt center is best described as a trigonally compressed octahedron with average angles of N-Co-N(A) = 91.40(2)° around the C_3 axis and N-Co-N(B) = 88.58(2)°.

Compound **2** was synthesized according to the reported procedure[28]. The structure of **2**, which was previously described,[28] contains a Co(II) center in a distorted trigonal prismatic environment (Figure 2) with three nitrogen atoms from the pyrazolyl moieties and an average distance Co-N(pz) of 2.065(1) Å and an average bite angle N(pz)-Co-N(pz) of 80.54(1)° along with three nitrogen atoms from the pyridine moieties with longer average distances of Co-N(py) = 2.274(1) Å and a wider average bite angle N(py)-Co-N(py) = 96.72(1)°.

Magnetic susceptibility measurements were performed on polycrystalline samples over the temperature range 1.8-300K under a 1000 Oe dc field. Room temperature χT values (3.17 emu.K.mol^{-1} for **1** and 2.85 emu.K.mol^{-1} for **2**) are higher than the spin-only values for an S = 3/2 center (1.87 emu/mol.K) as

[a] Department of Chemistry, Texas A&M University, College Station, TX 77842-3012 (USA). Fax: (+1) 979-845-7177. E-mail: dunbar@mail.chem.tamu.edu
[b] Chemistry Department, Faculty of Science, Fayoum University, Fayoum 63514, Egypt.

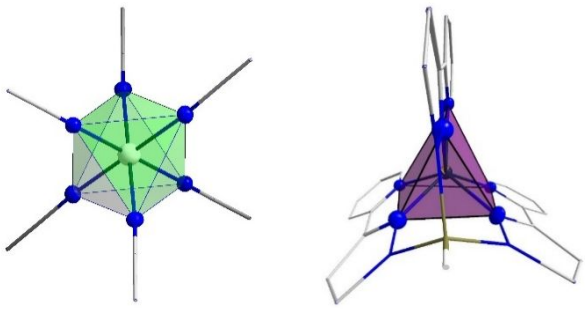

Figure 2. Molecular structure of $[Co(MeCN)_6]^{2+}$ in **1** (left) and $[CoTp^{py}]^{+}$ in **2** (right) with view along the C_3 axis. Ellipsoids are drawn at the 50% probability level and the hydrogen atoms were omitted for the sake of clarity.

expected due to the anisotropy of the cobalt ion in both complexes (Figure S2, S9). The much higher value for **1** is attributed to significant first-order unquenched orbital contributions due to orbital degeneracy in an octahedral symmetry. Upon lowering the temperature, the χT values for **1** exhibit a gradual decrease to 1.74 emu.K.mol^{-1} at 2K. In the case of **2**, χT remains constant down to ~100 K and then gradually decreases to 2.3 emu.K.mol^{-1} at 2K. The field dependent magnetization data were measured at fields up to 7 T and the resulting M versus H plots were observed to saturate at values well below that expected for an isotropic S = 3/2 ground state for both compounds, a consequence of magnetic anisotropy. The field dependence of the magnetization data at temperatures between 2 and 4.5 K for **1** exhibit non-superposition of the iso-field lines as expected for an anisotropic cobalt center (Figure S3) whereas the data for **2** do not show non-superposition which is not unprecedented for some highly anisotropic cobalt centers (S4).[8] The axial symmetry for both trigonal antiprismatic and trigonal prismatic geometries reflect significant unquenched first order orbital contributions which renders the zero-field splitting formalism (D, E) invalid for these systems. Thus, the χT data were fitted with PHI[29] according to the Hamiltonian:

$$\hat{H} = -\alpha\lambda\hat{L}\hat{S} + \alpha^2 B_2^0\left(\hat{L}_z^2 - \hat{L}^2\right) + \beta H(-\alpha\hat{L} + g_e\hat{S})$$

where α is the orbital reduction factor (~-1.5 for cobalt) and λ is the spin-orbit coupling constant (~-171.5 cm^{-1}). The best fits obtained for **1** indicate easy plane anisotropy with an axial crystal field parameter B_2^0 = +148.9 cm^{-1} and B_2^2 = ±44.5 cm^{-1} (g_x = 1.66, g_y = 2.4, g_z = 2.4). This type of anisotropy for **1** is unlike that of previously reported trigonal antiprismatic Co(II) SMMs,[17, 21-24] a fact that can be attributed to the compressed octahedral environment in **1** as compared to elongated geometries for other reported Co(II) SMMs. The large transverse anisotropy for **1** (B_2^2 = ±44.5 cm^{-1}) is expected to lead to significant quantum tunneling pathways that will efficiently quench the slow relaxation dynamics under a zero field. It is important to point out that several octahedral Co(II) mononuclear SMMs with a positive D value have been reported,[30, 31] with the spin relaxation being explained by considering hyperfine coupling and nuclear spin-lattice interactions which allow for phonon relaxation processes.[31-33]

Conversely, best fits for **2** indicate an easy axis anisotropy with B_2^0 = -156.2 cm^{-1} and B_2^2 = ±2 cm^{-1} (α = -1.5, λ = -171.5). Such large axial anisotropy in a trigonal prismatic environment has been reported to result in zero field slow relaxation phenomena (Table 1).

To investigate the dynamic magnetic properties, ac magnetic susceptibility data for **1** and **2** were measured as a function of both temperature and frequency under a zero applied external dc field. For compound **1,** no out-of-phase ac signal was observed under zero field which is attributed to significant quantum-tunneling of the magnetization (QTM) given the large transverse anisotropy (B_2^2 = ±44.5 cm^{-1}). In the case of compound **2**, a pronounced ac signal was observed under a zero applied field up to 18 K (Figure S10). Application of an external dc field to samples of **1** results in a field induced slow relaxation of the magnetization (Figure S6) whereas the ac signal in **2** is enhanced. In both cases, the field is expected to suppress quantum tunneling pathways. Variable-frequency ac data were measured at 1.8 K under applied dc fields in the range of 0 to 5000 Oe. The optimum signal was observed at 1500 Oe for **1**, and an optimum improvement in the relaxation time distribution was observed at 2000 Oe for **2** (S11). Variable-temperature (2.0-5.2 K) ac susceptibility data were collected under a 1500 Oe dc field for **1**, and under a zero field and a field of 2000 Oe (4.0-17 K) for **2** over the frequency range of 1-1500 Hz (Figure 3).

The Cole-Cole plots were fit to a Debye model (Figure S13). Fits to the Arrhenius law ($\tau = \tau_0 \exp(U_{eff}/k_B T)$) for the thermal relaxation pathway via an Orbach process (S14) were performed which led to effective energy barriers (U_{eff}) and pre-exponential factors (τ_0) of 8.6(1) cm^{-1} / 6.14(1) × 10^{-6} s for **1**; 36.2(1) cm^{-1} / 9.13(1)×10^{-6} s and 52.8(1) cm^{-1} / 1.56(1)×10^{-6} s for **2**, under a zero field and a 2000 Oe field respectively. Compound **2** was found to exhibit hysteresis, albeit waist-restricted, up to 3 K (Figure S14).

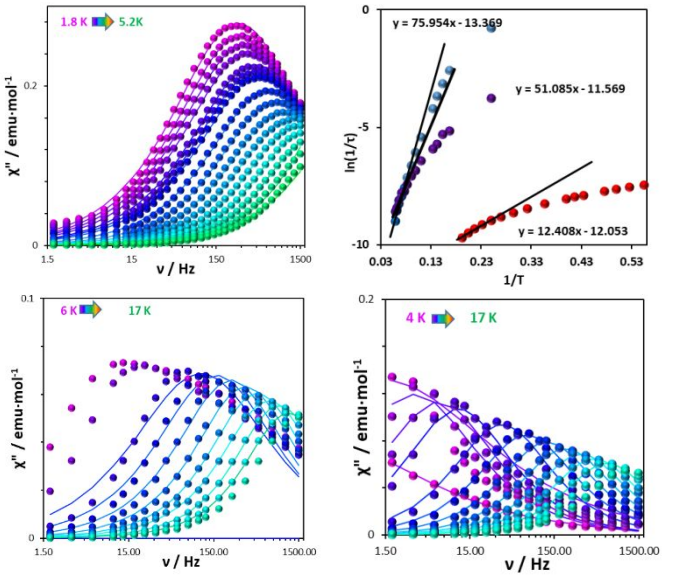

***Figure* 3**. Out-of-phase signal (χ") under a 1500 Oe applied dc field for **1** (top-left). Arrhenius fits of the energy barrier for **1** and **2** (top right). Out-of-phase signals (χ") for **2** under a zero applied field (bottom left) and under a 2000 Oe (bottom right)

Table 1. Magnetic parameters of trigonal prismatic and antiprismatic cobalt(II) SMMs

Compound	U_{eff} cm^{-1}	τ_0	B_2^0 cm^{-1}	*Zero field*	*ref*
$CoTp^*_2$	25.6	1.47 x 10^{-7}	-	no	[23]
$CoTp_2$	42.9	3.07 x 10^{-8}	-219	no	[24]
$[CoTpm_2](BPh_4)_2$	44.7	1 x10^{-7}	-92	no	[17]
$[CoTpm_2](ClO_4)_2$	33.6	2 x 10^{-7}	-93	no	[17]
$[Co(imidazole)_6][BPh_4]_2$	21.6	1.5 x 10^{-6}	-71	no	[22]
$[Co(MeCN)_6](BF_4)_2$ 1	7.6	8.3 x 10^{-6}	+148.9	no	This work
$[Co(P(S)\{[N(CH_3)NCHC_3N_2H_3]_3\})][(NO_3)_2]$	23	4 × 10^{-6}	−72(7)	yes	[6]
$(HNEt_3)(CoIICoIII_3L_6)$	75.7	1.7 × 10^{-7}	-115	yes	[7]
$[CoII(Pzox)_3(BC_6H_5)]Cl$	71	4.3 × 10^{-7}	- 82	yes	[8]
$[CoII(Pzox)_3(BC_{16}H_{33})]Cl$(β−Co)	109	2.65 × 10^{-9}	-111	yes	[9]
$[CoII(Pzox)_3(BC_{16}H_{33})]Cl$(α−Co)	180	8.87 × 10^{-10}		yes	[9]
[CoII(L)]	56.6	2.24 x10^{-10}	-31	yes	[10]
$(nBu_4N)[CoIICoIII_3(L5)_6]$ (8R)	102.8	2.5 × 10^{-8}	-	yes	[11]
$[CoII(Pzox)_3(BC_6H_5)]ClO_4$	101	-	-102.5	yes	[12]
$[Co(SDZ)_2bpy]$	35.2	4.61 × 10^{-8}	±81.6	no	[13]
$[Co(AcPyOx)_3BC_6H_5]ClO_4$	44.5	-	−95	yes	[14]
$(NBu_4)[Co(piv)_3]$	20.7	2.69 × 10^{-8}	−134.4	yes	[15]
$[Co(tppm)][ClO_4]_2{\cdot}2CH_3CN{\cdot}H_2O$	38.9	1.7 × 10^{-4}	−80.7	yes	[16, 18]
$[CoTp^{py}]PF_6$ (2)	52.8	1.56 x 10^{-6}	-156.5	yes	This work

The origins of the distinct magnetic behavior of **1** and **2** were probed by *ab initio* NEVPT2 calculations using the ORCA suite;[34] the methodology is described in the computational detail section. The calculated anisotropy parameters (B_2^0 and g-tensors) for both complexes are in excellent agreement with the experimental values (Table 2). The calculations indicate easy plane anisotropy for **1** (B_2^0 = +146.5 cm^{-1}) and axial anisotropy for **2** (B_2^0 = -150.6 cm^{-1}). For **1**, the lower three energy states are strongly multi-determinant (Figure S15).[35] The dominant electronic configurations for the ground state and the first and second excited states were found to be $(d_{xy})^2\{(d_{xz})(d_{yz})\}^3(d_{x^2-y^2})^1(d_{z^2})^1$ and $(d_{xy})^1\{(d_{xz})(d_{yz})\}^4(d_{x^2-y^2})^1(d_{z^2})^1$ respectively. For **1**, the major contributions to the positive B_2^0 value arise from ground-to-first and ground-to-second excited states transitions, both of which contribute equally to the total B_2^0 (Figure S15 and Table S3-4). These excitations occur between orbitals with different m_l values ($d_{xy} \rightarrow \{d_{xz}, d_{yz}\}$) which leads to a positive B_2^0 value.[36] For **2**, the dominant ground electronic configuration is $(d_{z^2})^2(d_{x^2-y^2})^2(d_{xy})^1(d_{xz})^1(d_{yz})^1$ which has a 51% contribution, whereas the first excited state is composed of several determinants with $(d_{z^2})^2(d_{x^2-y^2})^1(d_{xy})^2(d_{xz})^1(d_{yz})^1$ being the dominant electronic arrangement. In this case, the major contribution to B_2^0 arises from $d_{x^2-y^2} \rightarrow d_{xy}$ transitions (Figure S15 and Table S3-4). The ground to excited states contributions to the B_2^0 parameter can be correlated with the energy separation between these energy states ($\Delta E_{Root\ (1\text{-}2/1\text{-}3)}$). For **1**, the energy separation between the ground to first excited state is larger than it is for **2**, which leads to a nearly three-fold greater contribution to B_2^0 in the latter case (Table 2, Figure S15 and Table S3-4).

Anisotropy parameters (B_2^0, B_2^2 and g-tensors) together with transverse magnetic moments were also calculated for **1** and **2**

Table 2. NEVPT2-calculated (Orca) B_2^0 (cm^{-1}), g-tensor, the energy difference between ground and first two excited roots ($\Delta E_{Root\ (1\text{-}2/1\text{-}3)}$) along with CASSCF (MOLCAS) computed quantum tunneling of the magnetization (QTM) probabilities for **1** and **2**. The values in parentheses represent the calculated values from CASSCF calculations performed using MOLCAS.

	1	**2**
B_2^0 cm^{-1}	146.5 (154.8)	-150.6 (-149.5)
B_2^2 cm^{-1}	(-51.6)	(-0.5)
g_{xx}, g_{yy}, g_{zz}	1.741, 2.562, 2.563	1.352, 1.356, 3.513
	(1.848, 2.697, 2.319)	(1.698, 1.701, 3.597)
$\Delta E_{Root\ (1\text{-}2/1\text{-}3)}$ cm^{-1}	187.1, 187.6	25.6
QTM_{KD1} μ_B	(1.5)	(6.6X10^{-3})

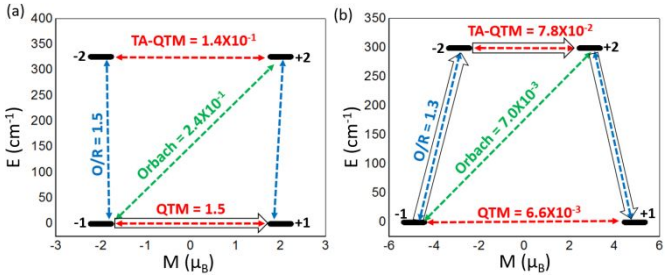

Figure 4. The *ab initio* SINGLE_ANISO computed magnetization blocking barrier for **1** (a) and **2** (b). The x-axis indicates the magnetic moment of each state along the main magnetic axis and the y-axis denotes the energy of the respective states. The thick black indicates Kramer's doublets as a function of the magnetic moment. The dotted green and blue lines indicate possible pathways of the Orbach and Orbach/Raman (O/R) contribution to the magnetic relaxation, respectively. The black arrows indicate the most suitable relaxation pathway for magnetization reorientation. The dotted red lines correspond to the QTM/TA-QTM relaxation pathways. The numbers provided at each arrow are the mean values for the corresponding matrix element of the magnetic moment.

using the MOLCAS suite.[37] The estimated magnitude and the sign of the B_2^0 and B_2^2 parameters for both compounds are in good agreement with the experimental data (Table 2). The computed B_2^2 parameter, which represents the transverse component of the anisotropy, is much larger for **1** than **2**, indicating more significant QTM for **1**. In the case of **1**, the computed transverse magnetic moments between the ground KD (QTM probability) and the Orbach process related to the ground state and the first excited state of opposite magnetization are very large (1.5 μ_B and 0.24 μ_B respectively, Figure 4). In contrast, these values are very small for **2** (6.6 x 10^{-3} μ_B and 7.8 x 10^{-2} μ_B respectively, Figure 4). These results explain why **1** exhibits field-induced SMM behaviour with a very small U_{eff} value and that **2** is a zero-field SMM.

Conclusions

The results reported herein underscore the importance of controlling local geometries of six-coordinate cobalt(II) centers. Detailed magneto-structural and theoretical studies of $[Co(MeCN)_6](BF_4)_2$ (**1**) and $[CoTp^{py}]PF_6$ (**2**), both of which are six-coordinate complexes with nitrogen donor ligands, revealed a significant transverse anisotropy (B_2^0 = +148.9 cm^{-1}, B_2^2 = ±44.5 cm^{-1}) and appreciable quantum tunnelling for **1** due to the non-rigid MeCN ligands in the distorted octahedral coordination environment. The rigid trigonal prismatic ligand framework in **2** leads to zero-field SMM behaviour due to easy axis anisotropy (B_2^0 = -150.5 cm^{-1}) with minimal transverse anisotropy component and quantum tunnelling as supported by *ab initio* CASSCF/NEVPT2 calculations.

Conflicts of interest

There are no conflicts to declare.

Notes and references

‡ KRD thanks the National Science Foundation (CHE-1808779) and the Welch Foundation (A-1449) for financial support. We are grateful to the HPRC at Texas A&M University for the computing resources.

§ Experimental and spectral data, and crystallographic data see ESI. Electronic Supplementary Information (ESI) available: See DOI: 10.1039/b000000x/.

1.D. Gatteschi and R. Sessoli, *Angew. Chem. Int. Ed. Eng*, 2003, **42**, 268-297.
2.J. M. Zadrozny, D. J. Xiao, M. Atanasov, G. J. Long, F. Grandjean, F. Neese and J. R. Long, *Nat Chem*, 2013, **5**, 577-581.
3.A. J. Brown, D. Pinkowicz, M. R. Saber and K. R. Dunbar, *Angew. Chem. Int. Ed.*, 2015, **54**, 5864-5868.
4.M. R. Saber and K. R. Dunbar, *Chem. Commun.*, 2014, **50**, 12266-12269.
5.J. J. Zhou, J. B. Song, A. H. Yuan, Z. X. Wang, L. Chen and Z. W. Ouyang, *Inorg. Chim. Acta*, 2018, **479**, 113-119.
6.S. Gomez-Coca, E. Cremades, N. Aliaga-Alcalde and E. Ruiz, *J. Am. Chem. Soc.*, 2013, **135**, 7010-7018.
7.Y. Y. Zhu, C. Cui, Y. Q. Zhang, J. H. Jia, X. Guo, C. Gao, K. Qian, S. D. Jiang, B. W. Wang, Z. M. Wang and S. Gao, *Chem. Sci.*, 2013, **4**, 1802-1806.
8.V. V. Novikov, A. A. Pavlov, Y. V. Nelyubina, M. E. Boulon, O. A. Varzatski, Y. Z. Voloshin and R. E. P. Winpenny, *J. Am. Chem. Soc.*, 2015, **137**, 9792-9795.
9.A. A. Pavlov, Y. V. Nelyubina, S. V. Kats, L. V. Penkova, N. N. Efimov, A. O. Dmitrienko, A. V. Vologzhanina, A. S. Belov, Y. Z. Voloshin and V. V. Novikov, *J. Phys. Chem. Lett.*, 2016, **7**, 4111-4116.
10.Y. Peng, T. Bodenstein, K. Fink, V. Mereacre, C. E. Anson and A. K. Powell, *Phys. Chem. Chem. Phys.*, 2016, **18**, 30135-30143.
11.Y. Y. Zhu, Y. Q. Zhang, T. T. Yin, C. Gao, B. W. Wang and S. Gao, *Inorg. Chem.*, 2015, **54**, 5475-5486.
12.A. A. Pavlov, D. Y. Aleshin, S. A. Savkina, A. S. Belov, N. N. Efimov, J. Nehrkorn, M. Ozerov, Y. Z. Voloshin, Y. V. Nelyubina and V. V. Novikov, *Chem. phys. chem*, 2019, **20**, 1001-1005.
13.C. Villa-Pérez, I. Oyarzabal, G. A. Echeverría, G. C. Valencia-Uribe, J. M. Seco and D. B. Soria, *Eur. J. Inorg. Chem.*, 2016, **2016**, 4835-4841.
14.A. A. Pavlov, S. A. Savkina, A. S. Belov, Y. V. Nelyubina, N. N. Efimov, Y. Z. Voloshin and V. V. Novikov, *Inorg. Chem.*, 2017, **56**, 6943-6951.
15.S. Y. Chen, H. H. Cui, Y. Q. Zhang, Z. X. Wang, Z. W. Ouyang, L. Chen, X. T. Chen, H. Yan and Z. L. Xue, *Dalton Trans.*, 2018, **47**, 10162-10171.
16.B. L. Yao, Y. F. Deng, T. R. Li, J. Xiong, B. W. Wang, Z. P. Zheng and Y. Z. Zhang, *Inorg. Chem.*, 2018, **57**, 14047-14051.
17.Y.-Z. Zhang, S. Gomez-Coca, A. J. Brown, M. R. Saber, X. Zhang and K. R. Dunbar, *Chem. Sci.*, 2016, **7** (10), 6519-6527.
18.B. Yao, M. K. Singh, Y.-F. Deng, Y.-N. Wang, K. R. Dunbar and Y.-Z. Zhang, *Inorg. Chem.*, 2020, DOI: 10.1021/acs.inorgchem.0c00950.
19.J. C. Hempel and M. E. Miller, *J. Chem. Phys.*, 1981, **75**, 2959-2970.
20.F. Lloret, M. Julve, J. Cano, R. Ruiz-Garcia and E. Pardo, *Inorg. Chim. Acta*, 2008, **361**, 3432-3445.
21.R. Mitsuhashi, K. S. Pedersen, T. Ueda, T. Suzuki, J. Bendix and M. Mikuriya, *Chem. Commun.*, 2018, **54**, 8869-8872.
22.L. Chen, J. J. Zhou, H. H. Cui, A. H. Yuan, Z. X. Wang, Y. Q. Zhang, Z. W. Ouyang and Y. Song, *Dalton Trans.*, 2018, **47**, 2506-2510.
23.J. Li, Y. Han, F. Cao, R. M. Wei, Y. Q. Zhang and Y. Song, *Dalton Trans.*, 2016, **45**, 9279-9284.
24.J. Zhang, J. Li, L. Yang, C. Yuan, Y. Q. Zhang and Y. Song, *Inorg. Chem.*, 2018, **57**, 3903-3912.
25.A. Switlicka, J. Palion-Gazda, B. Machura, J. Cano, F. Lloret and M. Julve, *Dalton Trans.*, 2019, **48**, 1404-1417.
26.Y. W. Wu, D. N. Tian, J. Ferrando-Soria, J. Cano, L. Yin, Z. W. Ouyang, Z. X. Wang, S. C. Luo, X. Y. Liu and E. Pardo, *Inorg. Chem. Front.*, 2019, **6**, 848-856.
27.B. J. Hathaway, D. G. Holah and A. E. Underhill, *J. Chem. Soc.*, 1962, 2444.
28.R. L. Paul, A. J. Amoroso, P. L. Jones, S. M. Couchman, Z. R. Reeves, L. H. Rees, J. C. Jeffery, J. A. McCleverty and M. D. Ward, *J. Chem. Soc., Dalton Trans.*, 1999, 1563-1568.
29.N. F. Chilton, R. P. Anderson, L. D. Turner, A. Soncini and K. S. Murray, *J. Comput. Chem.*, 2013, **34**, 1164-1175.
30.J. Vallejo, I. Castro, R. Ruiz-Garcia, J. Cano, M. Julve, F. Lloret, G. De Munno, W. Wernsdorfer and E. Pardo, *J. Am. Chem. Soc.*, 2012, **134**, 15704-15707.
31.S. Gómez-Coca, A. Urtizberea, E. Cremades, P. J. Alonso, A. Camón, E. Ruiz and F. Luis, *Nat. Commun.*, 2014, **5**.
32.D. H. Moseley, S. E. Stavretis, K. Thirunavukkuarasu, M. Ozerov, Y. Cheng, L. L. Daemen, J. Ludwig, Z. Lu, D. Smirnov, C. M. Brown, A. Pandey, A. J. Ramirez-Cuesta, A. C. Lamb, M. Atanasov, E. Bill, F. Neese and Z.-L. Xue, *Nat. Commun.*, 2018, **9**, 2572.
33.M. A. Hay, A. Sarkar, G. A. Craig, L. Bhaskaran, J. Nehrkorn, M. Ozerov, K. E. R. Marriott, C. Wilson, G. Rajaraman, S. Hill and M. Murrie, *Chem. Sci.*, 2019, **10**, 6354-6361.
34.F. Neese, *Wiley Interdiscip. Rev. Comput. Mol. Sc*, 2018, **8**, e1327.
35.P. C. Bunting, M. Atanasov, E. Damgaard-Møller, M. Perfetti, I. Crassee, M. Orlita, J. Overgaard, J. van Slageren, F. Neese and J. R. Long, *Science*, 2018, **362**, eaat7319.
36.M. K. Singh, P. Shukla, M. Khatua and G. Rajaraman, *Chem. Eur. J*, 2020, **26**, 464-477.
37.F. Aquilante, J. Autschbach, R. K. Carlson, L. F. Chibotaru, M. G. Delcey, L. De Vico, I. Fdez Galván, N. Ferré, L. M. Frutos, L. Gagliardi, M. Garavelli, A. Giussani, C. E. Hoyer, G. Li Manni, H. Lischka, D. Ma, P. Å. Malmqvist, T. Müller, A. Nenov, M. Olivucci, T. B. Pedersen, D. Peng, F. Plasser, B. Pritchard, M. Reiher, I. Rivalta, I. Schapiro, J. Segarra-Martí, M. Stenrup, D. G. Truhlar, L. Ungur, A. Valentini, S. Vancoillie, V. Veryazov, V. P. Vysotskiy, O. Weingart, F. Zapata and R. Lindh, *J. Comput. Chem.*, 2016, **37**, 506.

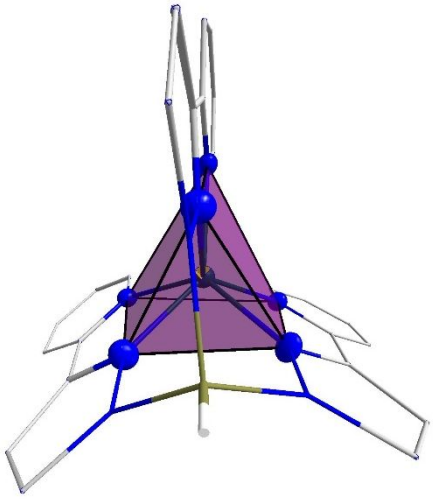

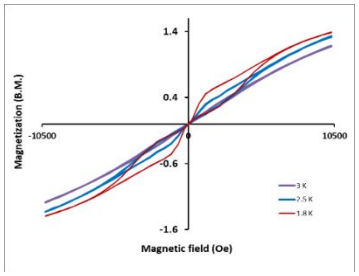

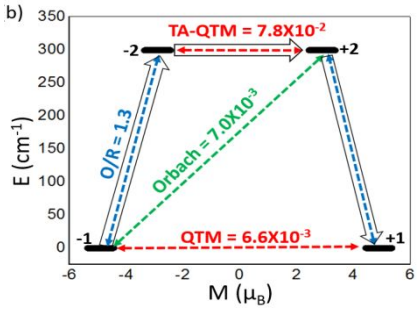

Suppression of quantum tunneling of the magnetization and zero-field SMM behavior was observed for the trigonal prismatic cobalt complex [CoTp^{py}]PF_6 (2) as evidenced by hysteresis up to 3K. Combined experimental and ab initio CASSCF/NEVPT2 calculations support the conclusion that the magnetic blocking in **2** is due to the enforced rigidity and axiality of the coordination environment.

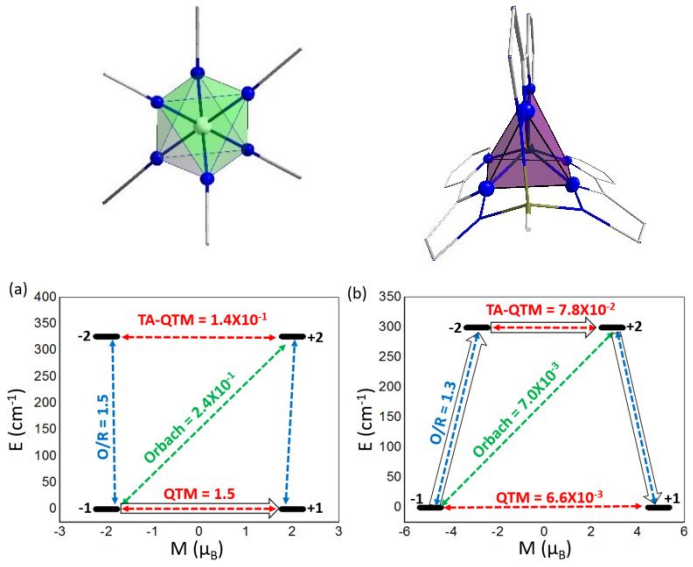

Combined experimental and ab initio CASSCF/NEVPT2 calculations revealed a significant transverse anisotropy (B_2^0 = +148.9 cm^{-1}, B_2^2 = ±44.5 cm^{-1}) and appreciable quantum tunnelling in $[Co(MeCN)_6](BF_4)_2$ (**1**) due to the non-rigid MeCN ligands in the distorted octahedral coordination environment. Suppression of quantum tunneling of the magnetization and subsequent zero-field SMM behavior was observed in the trigonal prismatic cobalt complex $[CoTp^{py}]PF_6$ (**2**) as evident by exhibiting hysteresis up to 3K. The improved magnetic blocking in **2** was attributed to the enforced rigidity and axiality of the coordination environment.